PERGAMON

International Journal of Heat and Mass Transfer 45 (2002) 3013–3032

International Journal of HEAT and MASS TRANSFER

www.elsevier.com/locate/ijhmt

Natural convection in three-dimensional porous cavities: integral transform method

H. Luz Neto [b], J.N.N. Quaresma [c], R.M. Cotta [a,*]

[a] *Mechanical Engineering Department, EE/COPPE/UFRJ, Universidade Federal do Rio de Janeiro, Cx. Postal 68503, Cidade Universitária, 21945-970 Rio de Janeiro, RJ, Brazil*

[b] *Instituto Nacional de Tecnologia, INT/MCT, Ministério de Ciência e Tecnologia, Rio de Janeiro, RJ, Brazil*

[c] *Chemical Engineering Department, DEQ/UFPA, Universidade Federal do Pará, Belém, PA, Brazil*

Received 31 May 2001; received in revised form 23 November 2001

Abstract

A transient three-dimensional Darcy model of natural convection in porous medium filled cavities is studied, using a vorticity-vector potential formulation and the generalized integral transform technique (GITT). A general formulation and solution methodology for vertical cavities (insulated vertical walls with differential horizontal wall temperatures) is developed. Results for cubic cavities are presented while evaluating the Rayleigh number effects for stable situations, observing the transient evolution of the heat transfer process. The convergence behavior of the proposed eigenfunction expansion solution is investigated and comparisons with previously reported steady-state solutions are critically performed.

Keywords: Natural convection; Porous media; Integral transforms; Computational methods; Unstable flows

1. Introduction

Heat transfer analysis in porous media is a key aspect in an ample range of applications, not only in natural media, such as rocks, sand layers and wood, but also in manufactured media, such as insulations and catalyzers, present in different processes in the chemical, mechanical, environmental and geological fields. Fundamentals and applications of heat and fluid flow within porous material filled enclosures are clearly and deeply presented in a number of well-established treatises such as [1–3].

Buoyancy induced flows in saturated porous media have been receiving considerable attention, due to the recognition that such flows can be quite influential in the operational characteristics of various systems, in both industrial and environmental applications. Such applications include, geothermal systems, petroleum reservoirs, fixed bed chemical reactors, cooling of nuclear reactors, building thermal insulation, grain drying, filtering processes, crystal growth, etc.

The technical literature is quite rich in terms of two-dimensional, steady or transient, treatments of natural convection in porous media, and the classical numerical techniques are quite developed in the solution of such mathematical formulations, under different flow models [1,3]. On the other hand, the analysis of three-dimensional problems is much more rare, especially for fully transient situations, mainly due to the sometimes prohibitive increase in computational effort associated with such purely discrete approaches. Some of the most relevant contributions to the objectives of the present analysis, in dealing with three-dimensional natural convection within porous cavities, are listed below [4–19]. The Darcy flow model is the most frequently adopted in these works, together with the assumptions of constant and isotropic physical properties and linear variation with temperature of the buoyancy term (Boussinesq approximation). Also, the cubic geometry is the most commonly treated one and the stable situation of a vertical

* Corresponding author. Tel.: +55-21-2562-8368; fax: +55-21-2290-6626.
E-mail address: renatocotta@hotmail.com (R.M. Cotta).

0017-9310/02/$ - see front matter
PII: S0017-9310(02)00015-7

Nomenclature

a	cavity width
b	cavity depth
c_p	specific heat
d	cavity height
Da	Darcy number, $Da = K/d^2$
g	gravity acceleration, $\boldsymbol{g} = (0, 0, -g)$
k_f	thermal conductivity of fluid
k_m	thermal conductivity of porous medium, $k_m = \Phi k_f + (1 - \Phi)k_s$
k_s	thermal conductivity of solid matrix
Mx	aspect ratio in x direction, $Mx = a/d$
My	aspect ratio in y direction, $My = b/d$
p	pressure – porous medium
P	dimensionless pressure, $P = Kp/(\alpha_m \mu)$
Pr	corrected Prandtl number – porous medium, $Pr = Pr_m \sigma$
Pr_f	fluid Prandtl number, $Pr_f = \nu/\alpha_f$
Pr_m	modified Prandtl number – porous medium, $Pr_m = \nu/\alpha_m$
Ra^*	Rayleigh number, $Ra^* = (\beta \Delta T g d^3)/(\nu \alpha_f)$
Ra	modified Rayleigh number – porous medium, $Ra = (\beta \Delta T g K d)/(\nu \alpha_m)$
t	time
T	temperature
v^*	fluid volumetric velocity, $\boldsymbol{v}^*(u^*, v^*, w^*)$
v	Darcy velocity field, $\boldsymbol{v}(u, v, w) = (d/\alpha_m)\boldsymbol{v}^*$
(x^*, y^*, z^*)	space coordinates
(x, y, z)	dimensionless coordinates, $x = x^*/d$, $y = y^*/d$, $z = z^*/d$

Greek symbols

α_f	fluid thermal diffusivity, $\alpha_f = k_f/(\rho c_p)_f$
α_m	solid matrix thermal diffusivity, $\alpha_m = k_m/(\rho c_p)_f$
β_f	fluid thermal expansion coefficient
Φ	porosity of solid matrix
K	permeability of solid matrix
μ	fluid absolute viscosity
ν	fluid kinematic viscosity, $\nu = \mu/\rho$
θ	dimensionless temperature, $\theta = (T - T_0)/\Delta T$, where $\Delta T = T_R - T_0$ with T_R and T_0 reference temperatures
θ_F	dimensionless filtering temperature, $\theta_F\ (x, y, z, \tau)$
θ_H	dimensionless filtered temperature, $\theta_H(x, y, z, \tau) = \sum_{i=0}^{\infty} \sum_{m=0}^{\infty} \sum_{q=1}^{\infty} F_i(x) G_m(y) H_q(z) \bar{\bar{\theta}}_{H_{imq}}(\tau)$
$\bar{\bar{\theta}}_{H_{imq}}$	transformed temperature field
ρ	fluid density, $\rho = \rho_f$
ρ_s	density of solid matrix
σ	thermal capacitance ratio, $\sigma = \chi/(\rho c_p)_f = (\rho c_p)_m/(\rho c_p)_f$
τ	dimensionless time, $\tau = \alpha_m t/(\sigma d^2) = k_m t/[(\rho c_p)_m d^2]$
Ξ	coefficient of transient term in momentum equations, $\Xi = Da/(\Phi Pr)$
ψ	vector potential, $\psi(\psi_x, \psi_y, \psi_z) = \nabla \times \boldsymbol{v}$
$\bar{\bar{\psi}}_{x_{imq}}$	transformed vector potential component, $\psi_x(x, y, z)$
$\bar{\bar{\psi}}_{y_{imq}}$	transformed vector potential component, $\psi_y(x, y, z)$

Subscripts

f	fluid
m	porous medium
s	solid matrix

enclosure, i.e., with a heated base and thermally insulated vertical walls, is frequently employed as the test case for the validation of solution methodologies.

Although most of the available contributions in three-dimensional heat and fluid flow simulation deal with the primitive variables formulation, the vorticity-vector potential approach has been receiving increasing attention. Aziz and Hellums [20], in a pioneering work, have shown that the vorticity-vector potential formulation could lead to more stable and fast simulations of three-dimensional flows. Later, Hirasaki and Hellums [21] provided a set of consistent boundary conditions for the vector potential, which were reasonably simple for confined flows. This contribution was then complemented by Hirasaki and Hellums [22], who employing the Helmholtz decomposition theorem, and introducing the concept of a scalar potential to the formulation, were able to reach simpler boundary conditions for the vector potential in every situation. This formulation was then applied to three-dimensional natural convection in porous media [4].

On the other hand, during the last two decades, a hybrid numerical–analytical approach for diffusion and convection–diffusion problems has been progressively advanced, towards the automatic error-controlled solution of such partial differential problems. This approach, known as the generalized integral transform technique (GITT) [23–25], derives its basis from the classical integral transform method for the exact solution of linear transformable diffusion problems. To illustrate some of the contributions on this method for the specific class of problems of interest here, we can mention the general solution for nonlinear convection–diffusion [26] and its extension to petroleum reservoir analysis [27], followed by the solution of a number of natural convection problems in cavities under steady and transient regime, for both porous media [28,29] or just fluid filled [30–33] two-dimensional enclosures. In all such contributions on natural convection, the streamfunction-only formulation was preferred, due to the inherent advantages in its combined use with this hybrid approach, as discussed in [34]. Later, this hybrid solution scheme was advanced to handle three-dimensional Navier–Stokes equations based on the vector–scalar potential formulation [35], with similar computational advantages with respect to the two-dimensional case.

The present contribution is aimed at advancing this computational tool towards the accurate solution of transient three-dimensional flows, here illustrated through laminar natural convection within porous media filled cavities. Adopting the Darcy flow model and the vorticity-vector potential formulation, a sufficiently general system of equations in the Cartesian coordinates system is considered, and the GITT is then applied to provide the hybrid numerical–analytical solution structure. This solution is then illustrated for the case of a cubic vertical cavity with differentially heated bottom and top walls, with insulated lateral walls, under stable flow patterns. The convergence behavior of the proposed solution is then thoroughly demonstrated and critically validated against previously reported numerical solutions, mostly for steady-state results. Finally, an analysis of the Rayleigh number influence in the transient three-dimensional heat and fluid flow phenomena is presented.

2. Problem formulation

Transient three-dimensional natural convection in a cavity filled with a porous material saturated with a Newtonian fluid is considered. The flow is buoyancy induced by heat exchange between the fluid-porous media and the

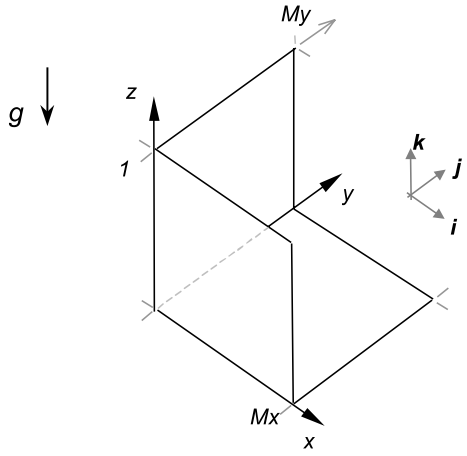

Fig. 1. Geometry and coordinates system for natural convection in a three-dimensional porous cavity.

impermeable walls. The geometric configuration considered (see Fig. 1) is known as the vertical cavity problem, in which boundary conditions of first kind, T_0 and $T_0 + \Delta T$, respectively, are imposed at the top and at the bottom walls, whilst the vertical walls are insulated. Within the validity of Darcy's law, and after invoking the Boussinesq approximation, this problem formulation in terms of primitive variables and in dimensionless form, is written as:

continuity equation:

$$\nabla \cdot \boldsymbol{v} = 0, \quad 0 < x < Mx, \ 0 < y < My, \ 0 < z < 1, \ \tau > 0, \tag{1}$$

momentum equation:

$$\frac{1}{\Phi}\frac{Da}{Pr}\frac{\partial \boldsymbol{v}}{\partial \tau} = -\nabla P + Ra\,\theta \boldsymbol{k} - \boldsymbol{v}, \quad 0 < x < Mx, \ 0 < y < My, \ 0 < z < 1, \ \tau > 0, \tag{2}$$

energy equation:

$$\frac{\partial \theta}{\partial \tau} + \boldsymbol{v} \cdot \nabla \theta = \nabla^2 \theta, \quad 0 < x < Mx, \ 0 < y < My, \ 0 < z < 1, \ \tau > 0, \tag{3}$$

subject to the following boundary conditions:

$$x = 0 \rightarrow \boldsymbol{v} = 0, \quad \frac{\partial \theta}{\partial x} = 0, \quad 0 < y < My, \quad 0 < z < 1, \quad \tau > 0, \tag{4a–d}$$

$$x = Mx \rightarrow \boldsymbol{v} = 0, \quad \frac{\partial \theta}{\partial x} = 0, \quad 0 < y < My, \quad 0 < z < 1, \quad \tau > 0, \tag{4e–h}$$

$$y = 0 \rightarrow \boldsymbol{v} = 0, \quad \frac{\partial \theta}{\partial y} = 0, \quad 0 < x < Mx, \quad 0 < z < 1, \quad \tau > 0, \tag{4i–l}$$

$$y = My \rightarrow \boldsymbol{v} = 0, \quad \frac{\partial \theta}{\partial y} = 0, \quad 0 < x < Mx, \quad 0 < z < 1, \quad \tau > 0, \tag{4m–p}$$

$$z = 0 \rightarrow \boldsymbol{v} = 0, \quad \theta = 1, \quad 0 < x < Mx, \quad 0 < y < My, \quad \tau > 0, \tag{4q–t}$$

$$z = 1 \rightarrow \boldsymbol{v} = 0, \quad \theta = 0, \quad 0 < x < Mx, \quad 0 < y < My, \quad \tau > 0, \tag{4u–x}$$

and with the initial conditions:

$$\tau = 0 \rightarrow \boldsymbol{v} = 0, \quad \theta = 0, \quad 0 \leqslant x \leqslant Mx, \quad 0 \leqslant y \leqslant My, \quad 0 \leqslant z \leqslant 1, \tag{5a–d}$$

where the following dimensionless groups were employed in Eqs. (1)–(5a–d) above:

$$x = \frac{x^*}{d}, \quad y = \frac{y^*}{d}, \quad z = \frac{z^*}{d}, \quad Mx = \frac{a}{d}, \quad My = \frac{b}{d}, \quad \boldsymbol{v} = \frac{d}{\alpha_{\mathrm{m}}}\boldsymbol{v}^*, \tag{6a–f}$$

$$\tau = \frac{k_{\mathrm{m}}}{(\rho c_{\mathrm{p}})_{\mathrm{m}} d^2} t = \frac{\alpha_{\mathrm{m}}}{\sigma d^2} t, \quad \theta = \frac{T - T_0}{\Delta T}, \quad P = \frac{K}{\alpha_{\mathrm{m}} \mu} p, \tag{6g–i}$$

$$Da = \frac{K}{d^2}, \quad Pr = \frac{\nu (\rho c_{\mathrm{p}})_{\mathrm{m}}}{k_{\mathrm{m}}} = \left[Pr = \frac{\nu}{k_{\mathrm{m}}/(\rho c_{\mathrm{p}})_{\mathrm{f}}} \sigma = Pr_{\mathrm{m}} \sigma \right], \quad Ra = \frac{\beta \Delta T g K d}{\nu \alpha_{\mathrm{m}}}, \tag{6j–l}$$

in which, $\Delta T = T_{\mathrm{R}} - T_0$, with T_0 and T_{R}, being reference temperatures, Da represents the Darcy number, Pr is the corrected Prandtl number, and Ra is the modified Rayleigh number for the porous medium.

3. Vorticity-vector potential formulation

In the solution of the above system, Eqs. (1)–(5a–d), via integral transformation, a first relevant observation is related to the pressure distribution, which acts as a source term in the momentum equations and is responsible for slower convergence rates in the expansions in terms of eigenfunctions. Another important aspect is concerned with the continuity equation, Eq. (1), which is expected to be identically satisfied for any truncation order in the expansions of the velocity components. One possible way of avoiding such difficulties, as an extension to the two-dimensional version, is to express Eqs. (1)–(5a–d) in terms of a vorticity-vector potential formulation. Thus, in order to make use of this formulation, the curl of Eq. (2) is taken, to yield

$$\frac{1}{\Phi}\frac{Da}{Pr}\frac{\partial\tilde{\omega}}{\partial\tau} = Ra\nabla\times\theta\boldsymbol{k} - \tilde{\omega}, \tag{7}$$

where $\tilde{\omega} = \nabla\times\boldsymbol{v}$ is the vorticity vector.

Then, the velocity field may be expressed in terms of a solenoid vector potential in the following way [20,21]:

$$\tilde{\omega} = \nabla\times\boldsymbol{v} = \nabla\times(\nabla\times\tilde{\boldsymbol{\psi}}) \equiv \nabla\times\underbrace{(\nabla\cdot\tilde{\boldsymbol{\psi}})}_{0} - (\nabla\cdot\nabla\tilde{\boldsymbol{\psi}}) = -\nabla^2\tilde{\boldsymbol{\psi}}. \tag{8}$$

Introducing Eq. (8) into Eq. (7), and performing the vector operations, yield

$$-\frac{1}{\Phi}\frac{Da}{Pr}\frac{\partial}{\partial\tau}(\nabla^2\tilde{\boldsymbol{\psi}}) = Ra\left[\frac{\partial\theta}{\partial y}\boldsymbol{i} - \frac{\partial\theta}{\partial x}\boldsymbol{j}\right] + \nabla^2\tilde{\boldsymbol{\psi}}. \tag{9}$$

Substituting the definition of the vector potential given by Eq. (8) into the energy equation, we obtain

$$\frac{\partial\theta}{\partial\tau} + (\nabla\times\tilde{\boldsymbol{\psi}})\cdot\nabla\theta = \nabla^2\theta. \tag{10}$$

Eqs. (9) and (10) are then decomposed to furnish the problem formulation in terms of the vector potential definition. The transient term in the momentum equations is in general neglected in dealing with stable Darcian flows. Then these governing equations for the vertical cavity can be rewritten as:

Momentum equations:

x-Component:

$$Ra\frac{\partial\theta}{\partial y} + \nabla^2\psi_x = 0, \quad 0 < x < Mx,\ 0 < y < My,\ 0 < z < 1,\ \tau > 0. \tag{11}$$

y-Component:

$$-Ra\frac{\partial\theta}{\partial x} + \nabla^2\psi_y = 0, \quad 0 < x < Mx,\ 0 < y < My,\ 0 < z < 1,\ \tau > 0. \tag{12}$$

Energy equation:

$$\frac{\partial\theta}{\partial\tau} - \frac{\partial\theta}{\partial x}\frac{\partial\psi_y}{\partial z} + \frac{\partial\theta}{\partial y}\frac{\partial\psi_x}{\partial z} + \frac{\partial\theta}{\partial z}\left[\frac{\partial\psi_y}{\partial x} - \frac{\partial\psi_x}{\partial y}\right] = \frac{\partial^2\theta}{\partial x^2} + \frac{\partial^2\theta}{\partial y^2} + \frac{\partial^2\theta}{\partial z^2}, \quad 0 < x < Mx,\ 0 < y < My,\ 0 < z < 1,\ \tau > 0. \tag{13}$$

Boundary conditions:

$$x = 0 \to \frac{\partial\psi_x}{\partial x} = \psi_y = 0, \quad \frac{\partial\theta}{\partial x} = 0, \quad 0 < y < My, \quad 0 < z < 1, \tag{14a–c}$$

$$x = Mx \to \frac{\partial\psi_x}{\partial x} = \psi_y = 0, \quad \frac{\partial\theta}{\partial x} = 0, \quad 0 < y < My, \quad 0 < z < 1, \tag{14d–f}$$

$$y = 0 \to \frac{\partial\psi_y}{\partial y} = \psi_x = 0, \quad \frac{\partial\theta}{\partial y} = 0, \quad 0 < x < Mx, \quad 0 < z < 1, \tag{14g–i}$$

$$y = My \to \frac{\partial\psi_y}{\partial y} = \psi_x = 0, \quad \frac{\partial\theta}{\partial y} = 0, \quad 0 < x < Mx, \quad 0 < z < 1, \tag{14j–l}$$

$$z = 0 \to \psi_x = \psi_y = 0, \quad \theta = 1, \quad 0 < x < Mx, \quad 0 < y < My, \tag{14m–o}$$

$$z = 1 \to \psi_x = \psi_y = 0, \quad \theta = 0, \quad 0 < x < Mx, \quad 0 < y < My. \tag{14p–r}$$

Initial conditions:

$$\tau = 0 \to \theta = 0, \quad 0 < x < Mx, \quad 0 < y < My, \quad 0 < z < 1. \tag{15}$$

It should be noted that the geometry and boundary conditions of the considered example, result in a vanishing z-component of the vector potential.

4. Solution methodology

Following the ideas in the solution methodology through the GITT approach [23–25], in order to make the boundary condition given by Eq. (14o) homogeneous, and thus enhance the computational performance of the eigenfunction expansions, the following filter for the temperature field, which is based on the solution of a steady-state pure heat conduction problem, is proposed:

$$\theta_F(z) = (1 - z), \tag{16}$$

then

$$\theta(x, y, z, \tau) = (1 - z) + \theta_H(x, y, z, \tau). \tag{17}$$

Eq. (17) is now employed by substituting it into Eqs. (11)–(15), so that the governing equations for the filtered potential θ_H are given as

$$Ra\frac{\partial \theta_H}{\partial y} + \nabla^2 \psi_x = 0, \quad 0 < x < Mx, \ 0 < y < My, \ 0 < z < 1, \ \tau > 0, \tag{18}$$

$$-Ra\frac{\partial \theta_H}{\partial x} + \nabla^2 \psi_y = 0, \quad 0 < x < Mx, \ 0 < y < My, \ 0 < z < 1, \ \tau > 0, \tag{19}$$

$$\frac{\partial \theta_H}{\partial \tau} - \frac{\partial \theta_H}{\partial x}\frac{\partial \psi_y}{\partial z} + \frac{\partial \theta_H}{\partial y}\frac{\partial \psi_x}{\partial z} + \frac{\partial \theta_H}{\partial z}\left[\frac{\partial \psi_y}{\partial x} - \frac{\partial \psi_x}{\partial y}\right] - \left[\frac{\partial \psi_y}{\partial x} - \frac{\partial \psi_x}{\partial y}\right] = \frac{\partial^2 \theta_H}{\partial x^2} + \frac{\partial^2 \theta_H}{\partial y^2} + \frac{\partial^2 \theta_H}{\partial z^2},$$
$$0 < x < Mx, \ 0 < y < My, \ 0 < z < 1, \ \tau > 0, \tag{20}$$

with the following boundary and initial conditions:

$$x = 0 \to \frac{\partial \psi_x}{\partial x} = \psi_y = 0, \quad \left(\frac{\partial \theta_H}{\partial x} = 0, \ \tau > 0\right), \quad 0 < y < My, \quad 0 < z < 1, \tag{21a–c}$$

$$x = Mx \to \frac{\partial \psi_x}{\partial x} = \psi_y = 0, \quad \left(\frac{\partial \theta_H}{\partial x} = 0, \ \tau > 0\right), \quad 0 < y < My, \quad 0 < z < 1, \tag{21d–f}$$

$$y = 0 \to \psi_x = \frac{\partial \psi_y}{\partial y} = 0, \quad \left(\frac{\partial \theta_H}{\partial y} = 0, \ \tau > 0\right), \quad 0 < x < Mx, \quad 0 < z < 1, \tag{21g–i}$$

$$y = My \to \psi_x = \frac{\partial \psi_y}{\partial y} = 0, \quad \left(\frac{\partial \theta_H}{\partial y} = 0, \ \tau > 0\right), \quad 0 < x < Mx, \quad 0 < z < 1, \tag{21j–l}$$

$$z = 0 \to \psi_x = \psi_y = 0, \quad (\theta_H = 0, \ \tau > 0), \quad 0 < x < Mx, \quad 0 < y < My, \tag{21m–o}$$

$$z = 1 \to \psi_x = \psi_y = 0, \quad (\theta_H = 0, \ \tau > 0), \quad 0 < x < Mx, \quad 0 < y < My, \tag{21p–r}$$

$$\tau = 0 \to \theta_H = -\theta_F, \quad 0 < x < Mx, \quad 0 < y < My, \quad 0 < z < 1. \tag{21s}$$

The next natural step in this solution methodology consists of the choice of appropriate eigenvalue problems, which shall provide the basis for the expansions of the original potentials, i.e., the components of the vector potential and the temperature field. Following previous developments [23,28], the eigenvalue problem for the ψ_x-component of the vector potential in the x direction is chosen as

$$\frac{d^2 \tilde{A}_i(x)}{dx^2} + \alpha_i^2 \tilde{A}_i(x) = 0, \quad 0 < x < Mx, \tag{22a}$$

$$\frac{d\tilde{A}_i(0)}{dx} = 0, \tag{22b}$$

$$\frac{d\tilde{A}_i(Mx)}{dx} = 0, \tag{22c}$$

with the respective solution for the eigenfunctions $\tilde{A}_i(x)$:

$$\tilde{A}_i(x) = \begin{cases} 1, & \alpha_i = 0, \ i = 0, \\ \cos(\alpha_i x), & \alpha_i = \frac{i\pi}{Mx}, \ i = 1, 2, 3, \ldots, \end{cases} \tag{22d, e}$$

satisfying the following orthogonality property:

$$\int_0^{Mx} \tilde{A}_i(x)\tilde{A}_j(x)\,\mathrm{d}x = \begin{cases} 0, & i \neq j, \\ NA_i, & i = j. \end{cases} \tag{22f, g}$$

The norm or normalization integral NA_i is obtained from

$$NA_i = \int_0^{Mx} \tilde{A}_i^2(x)\,\mathrm{d}x = \begin{cases} Mx, & i = 0, \\ Mx/2, & i = 1,2,3,\ldots \end{cases} \tag{22h, i}$$

The normalized eigenfunction is defined as

$$A_i(x) = \tilde{A}_i(x) \Big/ \sqrt{NA_i}, \quad i = 0,1,2,\ldots, \tag{22j}$$

which will provide a symmetric kernel in the integral transform pair.

Similar choices are made in the y and z directions, furnishing the following eigenquantities for this component of the vector potential, respectively:

$$\tilde{B}_\mathrm{m}(y) = \sin(\beta_\mathrm{m} y), \quad \beta_\mathrm{m} = \frac{m\pi}{My}, \quad m = 1,2,3,\ldots, \tag{23a, b}$$

$$\int_0^{My} \tilde{B}_\mathrm{m}(y)\tilde{B}_n(y)\,\mathrm{d}y = \begin{cases} 0, & m \neq n, \\ NB_\mathrm{m}, & m = n, \end{cases} \tag{23c, d}$$

$$NB_\mathrm{m} = \int_0^{My} \tilde{B}_\mathrm{m}^2(y)\,\mathrm{d}y = My/2, \quad m = 1,2,3,\ldots, \tag{23e}$$

$$B_\mathrm{m}(y) = \tilde{B}_\mathrm{m}(y) \Big/ \sqrt{NB_\mathrm{m}}, \quad m = 1,2,3,\ldots, \tag{23f}$$

and

$$\tilde{C}_q(z) = \sin(\gamma_q z), \quad \gamma_q = q\pi, \quad q = 1,2,3,\ldots, \tag{24a, b}$$

$$\int_0^1 \tilde{C}_q(z)\tilde{C}_n(z)\,\mathrm{d}y = \begin{cases} 0, & q \neq n, \\ NC_q, & q = n, \end{cases} \tag{24c, d}$$

$$NC_q = \int_0^1 \tilde{C}_q^2(z)\,\mathrm{d}z = 1/2, \quad q = 1,2,3,\ldots, \tag{24e}$$

$$C_q(z) = \tilde{C}_q(z) \Big/ \sqrt{NC_q}, \quad q = 1,2,3,\ldots \tag{24f}$$

The eigenfunctions, eigenvalues, orthogonality properties and norms associated with the ψ_y-component of the vector potential are given, respectively, by:

x-Direction:

$$\tilde{D}_i(x) = \sin(\delta_i x), \quad \delta_i = \frac{i\pi}{Mx}, \quad i = 1,2,3,\ldots, \tag{25a, b}$$

$$\int_0^{Mx} \tilde{D}_i(x)\tilde{D}_j(x)\,\mathrm{d}x = \begin{cases} 0, & i \neq j, \\ ND_i, & i = j, \end{cases} \tag{25c, d}$$

$$ND_i = \int_0^{Mx} \tilde{D}_i^2(x)\,\mathrm{d}x = Mx/2, \quad i = 1,2,3,\ldots, \tag{25e}$$

$$D_i(x) = \tilde{D}_i(x) \Big/ \sqrt{ND_i}, \quad i = 1,2,3,\ldots \tag{25f}$$

y-Direction:

$$\tilde{E}_\mathrm{m}(y) = \begin{cases} 1, & \varepsilon_\mathrm{m} = 0, \ m = 0, \\ \cos(\varepsilon_\mathrm{m} y), & \varepsilon_\mathrm{m} = \frac{m\pi}{My}, \ m = 1,2,3,\ldots, \end{cases} \tag{26a, b}$$

$$\int_0^{My} \tilde{E}_{\mathrm{m}}(y)\tilde{E}_n(y)\,\mathrm{d}y = \begin{cases} 0, & m \neq n, \\ NE_{\mathrm{m}}, & m = n, \end{cases} \tag{26c, d}$$

$$NE_{\mathrm{m}} = \int_0^{My} \tilde{E}_{\mathrm{m}}^2(y)\,\mathrm{d}y = \begin{cases} My, & m = 0, \\ My/2, & m = 1, 2, 3, \ldots, \end{cases} \tag{26e, f}$$

$$E_{\mathrm{m}}(y) = \tilde{E}_{\mathrm{m}}(y) \Big/ \sqrt{NE_{\mathrm{m}}}, \quad m = 1, 2, 3, \ldots \tag{26g}$$

z-Direction:

$$\tilde{C}_q(z) = \sin(\gamma_q z), \quad \gamma_q = q\pi, \ \ q = 1, 2, 3, \ldots, \tag{27a, b}$$

$$\int_0^1 \tilde{C}_q(z)\tilde{C}_n(z)\,\mathrm{d}y = \begin{cases} 0, & q \neq n, \\ NC_q, & q = n, \end{cases} \tag{27c, d}$$

$$NC_q = \int_0^1 \tilde{C}_q^2(z)\,\mathrm{d}z = 1/2, \quad q = 1, 2, 3, \ldots, \tag{27e}$$

$$C_q(z) = \tilde{C}_q(z) \Big/ \sqrt{NC_q}, \quad q = 1, 2, 3, \ldots \tag{27f}$$

For the temperature problem θ_H, the eigenquantities are given by:

x-Direction:

$$\tilde{A}_i(x) = \begin{cases} 1, & \alpha_i = 0, \ \ i = 0, \\ \cos(\alpha_i x), & \alpha_i = \frac{i\pi}{Mx}, \ \ i = 1, 2, 3, \ldots, \end{cases} \tag{28a, b}$$

$$\int_0^{Mx} \tilde{A}_i(x)\tilde{A}_j(x)\,\mathrm{d}x = \begin{cases} 0, & i \neq j, \\ NA_i, & i = j, \end{cases} \tag{28c, d}$$

$$NA_i = \int_0^{Mx} \tilde{A}_i^2(x)\,\mathrm{d}x = \begin{cases} Mx, & i = 0, \\ Mx/2, & i = 1, 2, 3, \ldots, \end{cases} \tag{28e, f}$$

$$A_i(x) = \tilde{A}_i(x) \Big/ \sqrt{NA_i}, \quad i = 0, 1, 2, \ldots \tag{28g}$$

y-Direction:

$$\tilde{E}_{\mathrm{m}}(y) = \begin{cases} 1, & \varepsilon_{\mathrm{m}} = 0, \ \ m = 0, \\ \cos(\varepsilon_{\mathrm{m}} y), & \varepsilon_{\mathrm{m}} = \frac{m\pi}{My}, \ \ m = 1, 2, 3, \ldots, \end{cases} \tag{29a, b}$$

$$\int_0^{My} \tilde{E}_{\mathrm{m}}(y)\tilde{E}_n(y)\,\mathrm{d}y = \begin{cases} 0, & m \neq n, \\ NE_{\mathrm{m}}, & m = n, \end{cases} \tag{29c, d}$$

$$NE_{\mathrm{m}} = \int_0^{My} \tilde{E}_{\mathrm{m}}^2(y)\,\mathrm{d}y = \begin{cases} My, & m = 0, \\ My/2, & m = 1, 2, 3, \ldots, \end{cases} \tag{29e, f}$$

$$E_{\mathrm{m}}(y) = \tilde{E}_{\mathrm{m}}(y) \Big/ \sqrt{NE_{\mathrm{m}}}, \quad m = 1, 2, 3, \ldots \tag{29g}$$

z-Direction:

$$\tilde{C}_q(z) = \sin(\gamma_q z), \quad \gamma_q = q\pi, \ \ q = 1, 2, 3, \ldots, \tag{30a, b}$$

$$\int_0^1 \tilde{C}_q(z)\tilde{C}_n(z)\,\mathrm{d}y = \begin{cases} 0, & q \neq n, \\ NC_q, & q = n, \end{cases} \tag{30c, d}$$

$$NC_q = \int_0^1 \tilde{C}_q^2(z)\,\mathrm{d}z = 1/2, \quad q = 1, 2, 3, \ldots, \tag{30e}$$

$$C_q(z) = \tilde{C}_q(z) \Big/ \sqrt{NC_q}, \quad q = 1, 2, 3, \ldots \tag{30f}$$

Following the formalism in the GITT, the triple transformations for the components of the vector potential and for the temperature field in the x, y and z directions are obtained from the integral transform pairs below:

ψ_x-Component:

$$\overline{\overline{\tilde{\psi}}}_{x_{imq}} = \int_0^{Mx}\int_0^{My}\int_0^{1} A_i(x)B_{\mathrm{m}}(y)C_q(z)\psi_x(x,y,z)\,\mathrm{d}x\,\mathrm{d}y\,\mathrm{d}z \quad \text{(transform)}, \tag{31a}$$

$$\psi_x(x,y,z) = \sum_{i=0}^{\infty}\sum_{m=1}^{\infty}\sum_{q=1}^{\infty} A_i(x)B_{\mathrm{m}}(y)C_q(z)\overline{\overline{\tilde{\psi}}}_{x_{imq}} \quad \text{(inverse)}. \tag{31b}$$

ψ_y-Component:

$$\overline{\overline{\tilde{\psi}}}_{y_{imq}} = \int_0^{Mx}\int_0^{My}\int_0^{1} D_i(x)E_{\mathrm{m}}(y)C_q(z)\psi_y(x,y,z)\,\mathrm{d}x\,\mathrm{d}y\,\mathrm{d}z \quad \text{(transform)}, \tag{32a}$$

$$\psi_y(x,y,z) = \sum_{i=1}^{\infty}\sum_{m=0}^{\infty}\sum_{q=1}^{\infty} D_i(x)E_{\mathrm{m}}(y)C_q(z)\overline{\overline{\tilde{\psi}}}_{y_{imq}} \quad \text{(inverse)}. \tag{32b}$$

Temperature field θ_H:

$$\overline{\overline{\tilde{\theta}}}_{H_{imq}}(\tau) = \int_0^{Mx}\int_0^{My}\int_0^{1} A_i(x)E_{\mathrm{m}}(y)C_q(z)\theta_H(x,y,z,\tau)\,\mathrm{d}x\,\mathrm{d}y\,\mathrm{d}z \quad \text{(transform)}, \tag{33a}$$

$$\theta_H(x,y,z,\tau) = \sum_{i=0}^{\infty}\sum_{m=0}^{\infty}\sum_{q=1}^{\infty} A_i(x)E_{\mathrm{m}}(y)C_q(z)\overline{\overline{\tilde{\theta}}}_{H_{imq}}(\tau) \quad \text{(inverse)}. \tag{33b}$$

Applying the triple transformations ((31a), (32a) and (33a)) in the vector potential and in the temperature problems, given by Eqs. (18), (19) and (20), respectively, results the following infinite coupled algebraic-ODE system:

$$\overline{\overline{\tilde{\psi}}}_{x_{imq}} = \frac{Ra}{(\alpha_i^2+\beta_{\mathrm{m}}^2+\gamma_q^2)}\sum_{n=0}^{\infty} f_{1_{mn}}\overline{\overline{\tilde{\theta}}}_{H_{inq}}(\tau), \quad i=0,1,2,\ldots,\ m=1,2,3,\ldots,\ q=1,2,3,\ldots, \tag{34a}$$

$$\overline{\overline{\tilde{\psi}}}_{y_{imq}} = -\frac{Ra}{(\delta_i^2+\varepsilon_{\mathrm{m}}^2+\gamma_q^2)}\sum_{j=0}^{\infty} f_{2_{ij}}\overline{\overline{\tilde{\theta}}}_{H_{jmq}}(\tau), \quad i=1,2,3,\ldots,\ m=0,1,2,\ldots,\ q=1,2,3,\ldots, \tag{34b}$$

$$\begin{aligned}
&\frac{\mathrm{d}\overline{\overline{\tilde{\theta}}}_{H_{imq}}(\tau)}{\mathrm{d}\tau} - \sum_{j=0}^{\infty}\sum_{n=0}^{\infty}\sum_{r=1}^{\infty}\sum_{k=1}^{\infty}\sum_{p=0}^{\infty}\sum_{s=1}^{\infty} f_{3_{ijk\,mnp\,qrs}}\overline{\overline{\tilde{\psi}}}_{y_{kps}}\overline{\overline{\tilde{\theta}}}_{H_{jnr}}(\tau) + \sum_{j=0}^{\infty}\sum_{n=0}^{\infty}\sum_{r=1}^{\infty}\sum_{k=0}^{\infty}\sum_{p=1}^{\infty}\sum_{s=1}^{\infty} f_{4_{ijk\,mnp\,qrs}}\overline{\overline{\tilde{\psi}}}_{x_{kps}}\overline{\overline{\tilde{\theta}}}_{H_{jnr}}(\tau)\\
&\quad + \sum_{j=0}^{\infty}\sum_{n=0}^{\infty}\sum_{r=1}^{\infty}\sum_{k=1}^{\infty}\sum_{p=0}^{\infty}\sum_{s=1}^{\infty} f_{5_{ijk\,mnp\,qrs}}\overline{\overline{\tilde{\psi}}}_{y_{kps}}\overline{\overline{\tilde{\theta}}}_{H_{jnr}}(\tau) - \sum_{j=0}^{\infty}\sum_{n=0}^{\infty}\sum_{r=1}^{\infty}\sum_{k=0}^{\infty}\sum_{p=1}^{\infty}\sum_{s=1}^{\infty} f_{6_{ijk\,mnp\,qrs}}\overline{\overline{\tilde{\psi}}}_{x_{kps}}\overline{\overline{\tilde{\theta}}}_{H_{jnr}}(\tau)\\
&\quad - \sum_{j=1}^{\infty}\sum_{n=0}^{\infty}\sum_{r=1}^{\infty} f_{7_{ij\,mn\,qr}}\overline{\overline{\tilde{\psi}}}_{y_{jnr}} + \sum_{j=0}^{\infty}\sum_{n=1}^{\infty}\sum_{r=1}^{\infty} f_{8_{ij\,mn\,qr}}\overline{\overline{\tilde{\psi}}}_{x_{jnr}} = -\left(\alpha_i^2+\varepsilon_{\mathrm{m}}^2+\gamma_q^2\right)\overline{\overline{\tilde{\theta}}}_{H_{imq}}(\tau),
\end{aligned} \tag{34c}$$

where

$$\beta_0 \equiv 0, \quad \delta_0 \equiv 0. \tag{34d,e}$$

The same transformation procedure is applied on the initial condition (21s), to furnish

$$\overline{\overline{\tilde{\theta}}}_{H_{imq}}(0) = \begin{cases} 0, & i\neq 0,\ m\neq 0,\ \forall q,\\ -\dfrac{\sqrt{2MxMy}}{\gamma_q}, & i=0,\ m=0,\ \forall q. \end{cases} \tag{34f,g}$$

The coefficients above are integrals of the related eigenfunctions, given by:

$$f_{1_{mn}} = \int_0^{My} B_{\mathrm{m}}(y)E_n'(y)\,\mathrm{d}y = -\varepsilon_{\mathrm{m}}, \quad f_{2_{ij}} = \int_0^{Mx} D_i(x)A_j'(x)\,\mathrm{d}x = -\alpha_i, \tag{35a}$$

$$f_{3_{ijk\,mnp\,qrs}} = \int_0^{Mx} A_i(x)A_j'(x)D_k(x)\,\mathrm{d}x\int_0^{My} E_{\mathrm{m}}(y)E_n(y)E_p(y)\,\mathrm{d}y\int_0^{1} C_q(z)C_r(z)C_{\mathrm{s}}'(z)\,\mathrm{d}z, \tag{35b}$$

$$f_{4_{ijk\,mnp\,qrs}} = \int_0^{Mx} A_i(x)A_j(x)A_k(x)\,\mathrm{d}x \int_0^{My} E_{\mathrm{m}}(y)E'_n(y)B_p(y)\,\mathrm{d}y \int_0^1 C_q(z)C_r(z)C'_{\mathrm{s}}(z)\,\mathrm{d}z, \tag{35c}$$

$$f_{5_{ijk\,mnp\,qrs}} = \int_0^{Mx} A_i(x)A_j(x)D'_k(x)\,\mathrm{d}x \int_0^{My} E_{\mathrm{m}}(y)E_n(y)E_p(y)\,\mathrm{d}y \int_0^1 C_q(z)C'_r(z)C_{\mathrm{s}}(z)\,\mathrm{d}z, \tag{35d}$$

$$f_{6_{ijk\,mnp\,qrs}} = \int_0^{Mx} A_i(x)A_j(x)A_k(x)\,\mathrm{d}x \int_0^{My} E_{\mathrm{m}}(y)E_n(y)B'_p(y)\,\mathrm{d}y \int_0^1 C_q(z)C'_r(z)C_{\mathrm{s}}(z)\,\mathrm{d}z, \tag{35e}$$

$$f_{7_{ij\,mn\,qr}} = \int_0^{Mx} A_i(x)D'_j(x)\,\mathrm{d}x \int_0^{My} E_{\mathrm{m}}(y)E_n(y)\,\mathrm{d}y \int_0^1 C_q(z)C_r(z)\,\mathrm{d}z, \tag{35f}$$

$$f_{8_{ij\,mn\,qr}} = \int_0^{Mx} A_i(x)A_j(x)\,\mathrm{d}x \int_0^{My} E_{\mathrm{m}}(y)B'_n(y)\,\mathrm{d}y \int_0^1 C_q(z)C_r(z)\,\mathrm{d}z. \tag{35g}$$

Substituting Eqs. (34a) and (34b) into Eq. (34c), the following nonlinear ODE system, to determine the transformed potentials $\overline{\overline{\theta}}_{H_{imq}}$ for the temperature field, is obtained:

$$\frac{\mathrm{d}\overline{\overline{\theta}}_{H_{imq}}(\tau)}{\mathrm{d}\tau} + \sum_{j=0}^{\infty}\sum_{n=0}^{\infty}\sum_{r=1}^{\infty}\left\{\sum_{k=0}^{\infty}\sum_{p=0}^{\infty}\sum_{s=1}^{\infty}\left[W_{ijk\,mnp\,qrs}\right]\overline{\overline{\theta}}_{H_{kps}}(\tau)\right\}\overline{\overline{\theta}}_{H_{jnr}}(\tau) + Q_{imq}\overline{\overline{\theta}}_{H_{imq}}(\tau) = 0, \tag{36a}$$

$$\overline{\overline{\theta}}_{H_{imq}}(0) = \begin{cases} 0, & i \neq 0,\ \ m \neq 0,\ \ \forall q, \\ -\dfrac{\sqrt{2MxMy}}{\gamma_q}, & i = 0,\ \ m = 0,\ \ \forall q, \end{cases} \tag{36b, c}$$

where

$$W_{ijk\,mnp\,qrs} = (f_{5_{ijk\,mnp\,qrs}} - f_{3_{ijk\,mnp\,qrs}})\frac{Ra\,\alpha_k}{(\delta_k^2 + \varepsilon_p^2 + \gamma_{\mathrm{s}}^2)} + (f_{6_{ijk\,mnp\,qrs}} - f_{4_{ijk\,mnp\,qrs}})\frac{Ra\,\varepsilon_p}{(\alpha_k^2 + \beta_p^2 + \gamma_{\mathrm{s}}^2)}, \tag{37a}$$

$$Q_{imq} = (\alpha_i^2 + \varepsilon_{\mathrm{m}}^2 + \gamma_q^2) - \frac{Ra\,\alpha_i\delta_i}{(\delta_i^2 + \varepsilon_{\mathrm{m}}^2 + \gamma_q^2)} - \frac{Ra\,\beta_{\mathrm{m}}\varepsilon_{\mathrm{m}}}{(\alpha_i^2 + \beta_{\mathrm{m}}^2 + \gamma_q^2)}. \tag{37b}$$

The related coefficients given by Eqs. (35a)–(35g) above are analytically handled through symbolic manipulation packages [36], and the details in determination of these coefficients can be found in [37]. The symbolic expressions are then automatically converted to Fortran form, as made possible by a specific command in the *Mathematica* system [37], considerably simplifying both the analysis task and the computer code construction.

Eqs. (36a) and (36b,c) form an infinite system of coupled nonlinear ODEs, to be solved for the transformed potentials of the temperature field. Only the truncated version of such system can be actually solved. However, the direct truncation of the involved summations in this system at a specified order may not be efficient for computational purposes, since this approach can include some terms that are not important in the convergence criteria imposed by the user prescribed accuracy. A way of avoiding this difficulty is to transform the triple summations to single ones according to an appropriate reordering scheme, such as shown in [38,39] for multidimensional eigenfunction expansions. Here, the criteria adopted for the ordering procedure involves the summation of the squared eigenvalues in each direction as

$$\widehat{\alpha}_{\hat{i}}^2 = (\alpha_i^2 + \beta_{\mathrm{m}}^2 + \gamma_q^2) = (\delta_i^2 + \varepsilon_{\mathrm{m}}^2 + \gamma_q^2) = (\alpha_i^2 + \varepsilon_{\mathrm{m}}^2 + \gamma_q^2) = \pi^2\left(\frac{i^2}{Mx^2} + \frac{m^2}{My^2} + q^2\right). \tag{38a}$$

Then, the indices i, m and q are related to a single one $\hat{i}$ as

$$i = I(\hat{i}), \quad m = M(\hat{i}), \quad q = Q(\hat{i}), \tag{38b–d}$$

where $I(\hat{x}), M(\hat{x}), Q(\hat{x})$ are ordering arrays. The associated triple summations are then rewritten as a single one according to Eqs. (38b–d).

Similarly, as the ordering criteria is the same, we have

$$j = I(\hat{j}), \quad n = M(\hat{j}), \quad r = Q(\hat{j}), \tag{38e–g}$$

$$k = I(\hat{k}), \quad p = M(\hat{k}), \quad s = Q(\hat{k}), \tag{38h–i}$$

with the consideration of the following index reorganization:

$$\sum_{i}\sum_{\mathrm{m}}\sum_{q}\Rightarrow\sum_{\widehat{i}},\quad \sum_{j}\sum_{n}\sum_{r}\Rightarrow\sum_{\widehat{j}}\quad\text{and}\quad \sum_{k}\sum_{p}\sum_{\mathrm{s}}\Rightarrow\sum_{\widehat{k}}.$$

System (36a) and (36b,c) is then rewritten in the more compact and computationally efficient form:

$$\frac{\mathrm{d}\bar{\bar{\theta}}_{H_i}(\tau)}{\mathrm{d}\tau}+\sum_{j=1}^{\infty}\left[\sum_{k=1}^{\infty}W_{ijk}\bar{\bar{\theta}}_{H_k}(\tau)\right]\bar{\bar{\theta}}_{H_j}(\tau)+Q_i\bar{\bar{\theta}}_{H_i}(\tau)=0,\quad \widehat{i}=1,2,3,\ldots, \tag{39a}$$

$$\bar{\bar{\theta}}_{H_i}(0)=\begin{cases}0, & i\neq 0,\ m\neq 0,\ \forall q,\\ -\frac{\sqrt{2MxMy}}{\gamma_q}, & i=0,\ m=0,\ \forall q,\end{cases} \tag{39b, c}$$

where

$$W_{ijk}=\frac{Ra}{\widehat{\alpha}^2_{k}}[\alpha_k f_{53_{ijk}}+\varepsilon_p f_{64_{ijk}}], \tag{40a}$$

$$Q_i=\widehat{\alpha}^2_{i}-Ra\frac{\alpha_i^2+\varepsilon_{\mathrm{m}}^2}{\widehat{\alpha}^2_{i}}, \tag{40b}$$

and

$$f_{53_{ijk}}=f_{5_{ijk}}-f_{3_{ijk}}, \tag{40c}$$

$$f_{64_{ijk}}=f_{6_{ijk}}-f_{4_{ijk}}, \tag{40d}$$

$$\beta_0\equiv 0,\quad \delta_0\equiv 0. \tag{40e–f}$$

System (39a) and (39b,c) is now in the appropriate format for numerical solution through dedicated routines for initial value problems, such as the subroutines DIVPAG or DIVPRK from the IMSL Library [40], which are well tested and capable of handling such situations, offering an automatic accuracy control scheme. For this computational purpose, the expansions are then truncated to NT terms, so as to reach the user requested accuracy target in the final solution.

From the solution of system (39a) and (39b,c) above, the components of the vector potential and the temperature field, as well as other quantities of practical interest, are then readily obtained from the inversion formulae (31b), (32b) and (33b), in the form:

$$\psi_x(x,y,z)=-Ra\sum_{\widehat{i}=1}^{NT}\frac{\varepsilon_{m(\widehat{i})}}{\widehat{\alpha}^2_{\widehat{i}}}A_{i(\widehat{i})}(x)B_{m(\widehat{i})}(y)C_{q(\widehat{i})}(z)\bar{\bar{\theta}}_{H_{\widehat{i}}}(\tau), \tag{41a}$$

$$\psi_y(x,y,z)=Ra\sum_{\widehat{i}=1}^{NT}\frac{\alpha_{i(\widehat{i})}}{\widehat{\alpha}^2_{\widehat{i}}}D_{i(\widehat{i})}(x)E_{m(\widehat{i})}(y)C_{q(\widehat{i})}(z)\bar{\bar{\theta}}_{H_{\widehat{i}}}(\tau), \tag{41b}$$

$$\theta_H(x,y,z,\tau)=\sum_{\widehat{i}=1}^{NT}A_{i(\widehat{i})}(x)E_{m(\widehat{i})}(y)C_{q(\widehat{i})}(z)\bar{\bar{\theta}}_{H_{\widehat{i}}}(\tau), \tag{41c}$$

$$\theta(x,y,z,\tau)=(1-z)+\theta_H(x,y,z,\tau)=(1-z)+\sum_{\widehat{i}=1}^{NT}A_{i(\widehat{i})}(x)E_{m(\widehat{i})}(y)C_{q(\widehat{i})}(z)\bar{\bar{\theta}}_{H_{\widehat{i}}}(\tau). \tag{41d}$$

From the definitions for the local and overall Nusselt numbers, we obtain:

Local Nusselt number:

$$Nu(x,y,\tau)|_{z=\breve{z}}=-\left.\frac{\partial\theta}{\partial z}\right|_{z=\breve{z}}, \tag{42}$$

then

$$\left.\frac{\partial\theta}{\partial z}\right|_{z=\breve{z}}=\sum_{\widehat{i}=1}^{NT}\left[A_{i(\widehat{i})}(x)E_{m(\widehat{i})}(y)\left.\frac{\mathrm{d}C_{q(\widehat{i})}(z)}{\mathrm{d}z}\right|_{z=\breve{z}}\bar{\bar{\theta}}_{H_{\widehat{i}}}(\tau)\right]-1, \tag{43a}$$

$$A_{i(\widehat{i})}(x)=\begin{cases}\frac{1}{Mx^{1/2}}, & i(\widehat{i})=0,\\ \sqrt{\frac{2}{Mx}}\cos\left(\frac{i(\widehat{i})\pi}{Mx}x\right), & i(\widehat{i})\neq 0,\end{cases} \tag{43b, c}$$

$$E_{m(\widehat{i})}(y)=\begin{cases}\frac{1}{My^{1/2}}, & m(\widehat{i})=0,\\ \sqrt{\frac{2}{My}}\cos\left(\frac{m(\widehat{i})\pi}{My}y\right), & m(\widehat{i})\neq 0,\end{cases} \tag{43d, e}$$

$$\frac{\mathrm{d}C_{q(\widehat{i})}(z)}{\mathrm{d}z}=\begin{cases}\sqrt{2}q(\widehat{i})\pi, & z=0,\\ (-1)^{q(\widehat{i})}\sqrt{2}q(\widehat{i})\pi, & z=1.\end{cases} \tag{43f, g}$$

Overall Nusselt number:

$$\overline{Nu}(\tau)\big|_{z=\breve{z}}=-\int_0^{Mx}\int_0^{My}\frac{\partial\theta}{\partial z}\bigg|_{z=\breve{z}}\mathrm{d}y\,\mathrm{d}x, \tag{44a}$$

where

$$\overline{Nu}(\tau)\big|_{z=\breve{z}}=MxMy-\sum_{\widehat{i}=1}^{NT}\left[\int_0^{Mx}A_{i(\widehat{i})}(x)\,\mathrm{d}x\int_0^{My}E_{m(\widehat{i})}(y)\,\mathrm{d}y\frac{\mathrm{d}C_{q(\widehat{i})}(z)}{\mathrm{d}z}\bigg|_{z=\breve{z}}\bar{\bar{\theta}}_{H_{\widehat{i}}}(\tau)\right], \tag{44b}$$

$$\int_0^{Mx}A_{i(\widehat{i})}(x)\,\mathrm{d}x=\begin{cases}Mx^{1/2}, & i(\widehat{i})=0,\\ \frac{\sqrt{2Mx}}{i(\widehat{i})\pi}\sin\left(\frac{i(\widehat{i})\pi}{Mx}x\right)\Big|_0^{Mx}=0, & i(\widehat{i})\neq 0,\end{cases} \tag{44c, d}$$

$$\int_0^{My}E_{m(\widehat{i})}(y)\,\mathrm{d}y=\begin{cases}My^{1/2}, & m(\widehat{i})=0,\\ \frac{\sqrt{2My}}{m(\widehat{i})\pi}\sin\left(\frac{m(\widehat{i})\pi}{My}y\right)\Big|_0^{My}=0, & m(\widehat{i})\neq 0,\end{cases} \tag{44e, f}$$

$$\frac{\mathrm{d}C_{q(\widehat{i})}(z)}{\mathrm{d}z}=\begin{cases}\sqrt{2}q(\widehat{i})\pi, & z=0,\\ (-1)^{q(\widehat{i})}\sqrt{2}q(\widehat{i})\pi, & z=1.\end{cases} \tag{44g, h}$$

5. Results and discussion

This section illustrates some of the numerical results achieved from the computer code in Fortran, executed under a Pentium III 650 MHz platform. The subroutine DIVPRK of the IMSL Library [40] was employed for the transformed

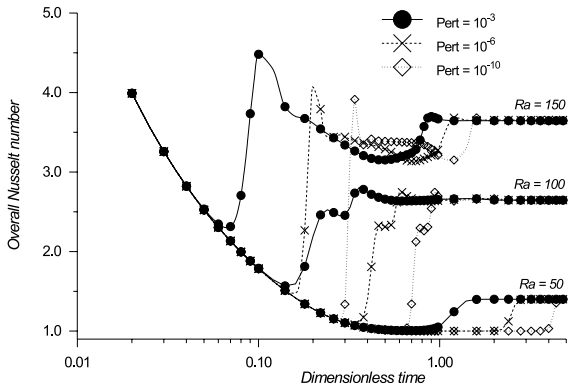

Fig. 2. Effect of initial condition perturbation on transient behavior – cubic cavity: TOL = 10^{-6}.

system solution, always with a relative error target of 10^{-6}. Before presenting a parametric analysis for the cubic cavity situation, aspects such as the influence of the initial condition perturbation, convergence analysis and covalidation are addressed.

As pointed out before [41], application of the classical Darcy model to the vertical cavity problem above described, directly leads to the pure conduction solution. For the convection regime to be triggered, a perturbation has to be introduced in the governing equations. Therefore, we first analyze the influence of the initial condition perturbation here proposed, on the system transient behavior. This analysis was accomplished considering four levels of perturbation for three different Rayleigh numbers. Fig. 2 illustrates such results, in terms of the overall Nusselt number as a function of dimensionless time, which have a similar nature to those described in the two-dimensional situation [41], showing that the elimination of the transient term in the flow equations tends to shift the onset of the convection regime to infinity.

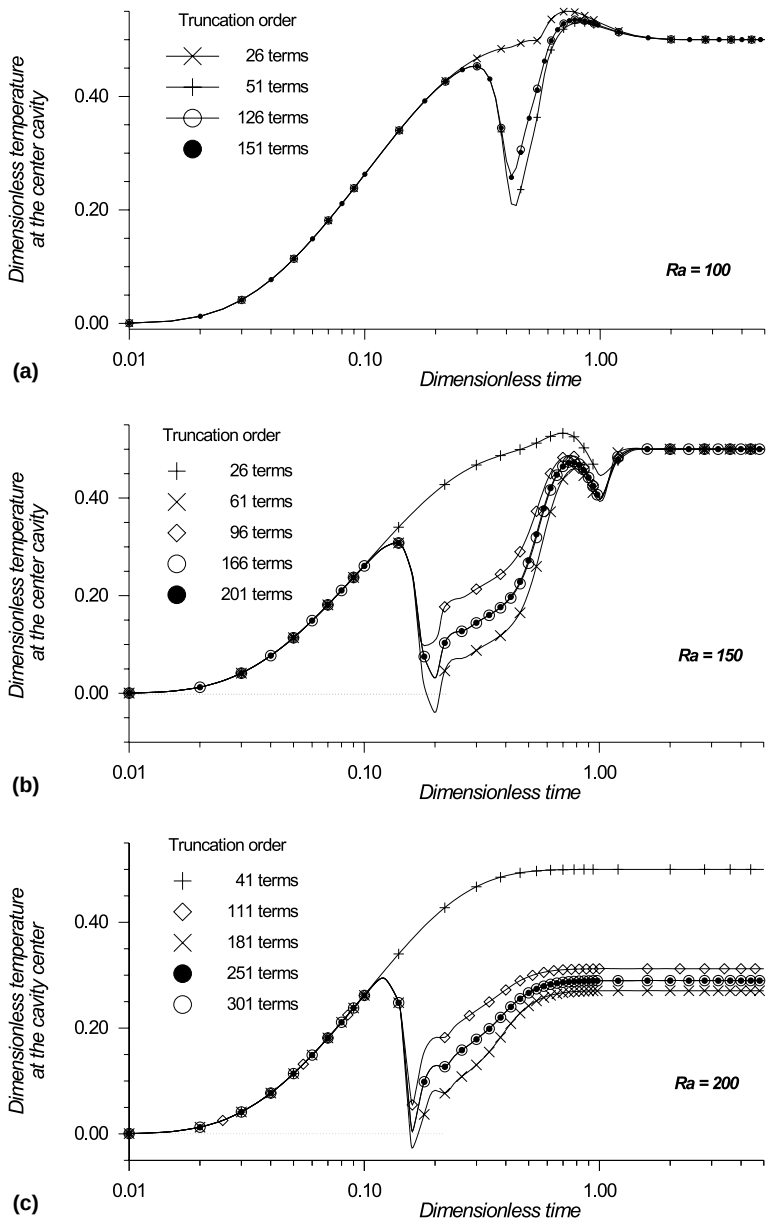

Fig. 3. Convergence of transient temperature at the cavity center ($Ra = 100$, 150, and 200): PERT $= 10^{-6}$, TOL $= 10^{-6}$.

Thus, it is quite clear that the quasi-steady Darcy flow model cannot in fact predict the actual transient behavior in the present physical situation, but rather offers information on its qualitative behavior and reproduces the desired steady-state solution, after the convection regime is triggered by the initial condition perturbation. In the following analysis, a value of the initial condition perturbation of PERT $= 10^{-6}$ was employed throughout.

The next step is the convergence analysis of the proposed eigenfunction expansions. Since the analytical expression for the overall Nusselt number is obtained through an integral balance procedure, its convergence is much more favorable than the original temperature field expansion. Therefore, convergence was directly analyzed over the temperature evolution results, at different selected points within the cavity.

Fig. 3 illustrates the convergence of the transient temperature distribution at the cavity center for different values of the Rayleigh number, $Ra = 100$, 150 and 200, for different truncation orders in the eigenfunction expansion. To the graph scale the convergence is quite favorable, with higher values of Ra requiring higher truncation orders, as expected, due to the increased importance of the convective source terms. A tabular form of these results was also inspected, leading to the conclusion that three fully converged significant digits could be achieved within practical limits of computational effort, in all cases considered. It should be pointed out, however, that very low truncation orders may not capture the actual transient behavior in the region where the convective regime is triggered.

We now proceed towards the covalidation of the proposed approach against previously reported results in the literature. There is an evident lack of fully transient results in previous contributions for the present physical situation, which limits the present comparisons to steady-state values of the overall Nusselt number. The pioneering work of Holst and Aziz [4] was included in this covalidation effort especially due to its theoretical value, that in fact allowed for the present implementation, but it should be recalled that computational resources at that time were quite a limiting factor in multidimensional simulations. The basis for comparison was the more recent contribution of Stamps et al. [16], in 1990, who also followed the work in [4] and employed the ADI method for the parabolic problem and the SOR scheme for the elliptic portions, both with second-order finite differences, including the boundaries.

Fig. 4 presents an ample comparison of the steady-state overall Nusselt numbers, including different implementations reviewed within Section 1. The continuous line represents a polynomial fit to the present results, while specific numerical results are emphasized at selected values of Ra. The overall agreement is indeed quite satisfactory considering the difficulty of the computational task involved, and the different formulations and solution methodologies employed. Except for the case of $Ra = 50$, the direct comparison with the tabulated results of Stamps et al. [16] yields agreements of two or even three significant digits. However, it will be clear in what follows that we would need the information on the dimensionless time at which these results were extracted from the transient or pseudo-transient solution, so as to guarantee a more proper comparison.

As an additional validation of the proposed code, Fig. 5 demonstrates the satisfaction of the global energy balance, by presenting the transient evolution of the average Nusselt numbers at the bottom and top walls of the cavity. The merging of these curves as the steady state is approached, for different values of Rayleigh number, provides further confidence on the appropriate choice of basis and algorithm construction.

The present methodology is now employed in the analysis of the convective phenomena within cubic cavities, by studying the transient behavior of the overall Nusselt number in terms of the Rayleigh number, which was varied from

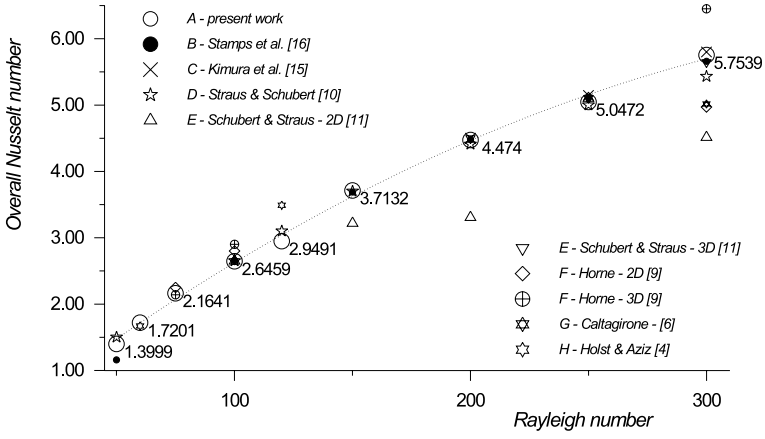

Fig. 4. Covalidation of steady overall Nusselt numbers – cubic cavity.

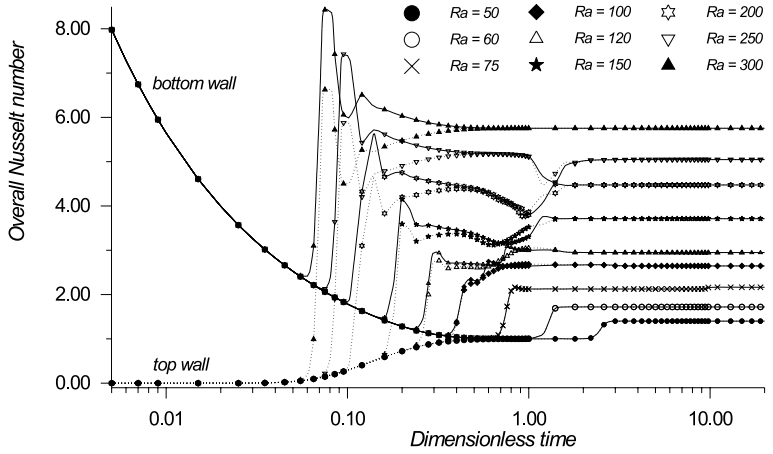

Fig. 5. Verification of overall energy balance satisfaction.

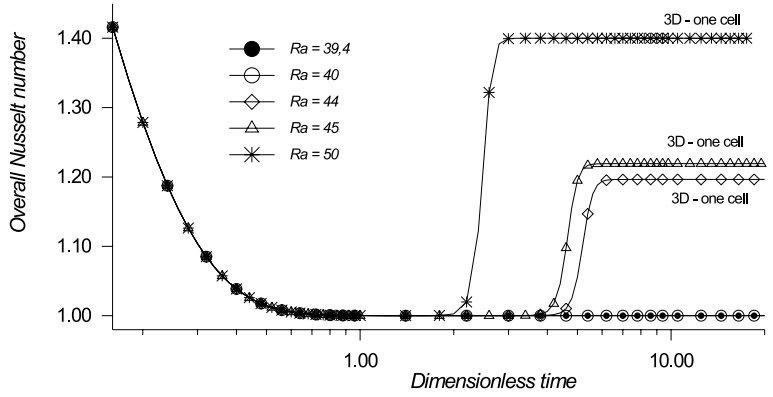

Fig. 6. Transient behavior of overall Nusselt number – cubic cavity: $Ra = 39.4$, 40, 45 and 50.

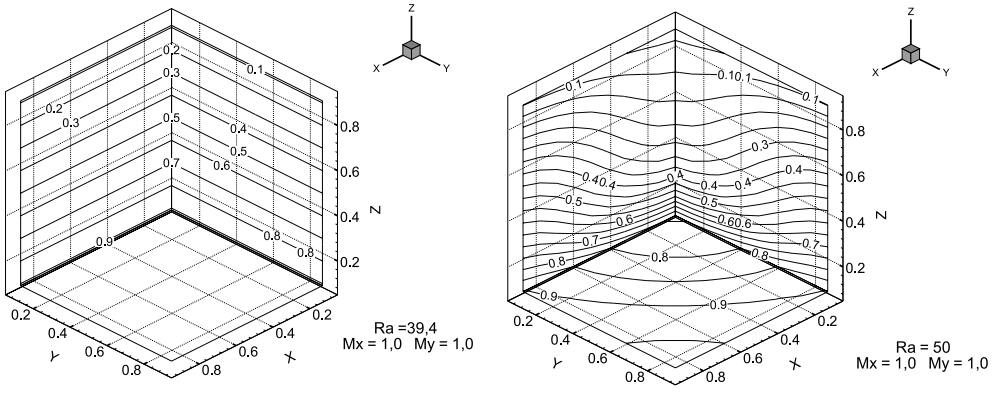

Fig. 7. Isolines of temperature at the rear faces of the cavity – steady state – cubic cavity: $Ra = 39.4$ and 50.

an initial value of less than the lowest critical value, $4\pi^2$, up to the higher value of 300 when the stability of the convective process can still be warranted. The maximum dimensionless time prescribed within the simulations was $\tau = 20$.

Fig. 6 presents the evolution of the overall Nusselt numbers for $Ra = 39.4$, 40, 44, 45 and 50, where the convective regime finally achieved in each case is indicated. It was then verified that for $Ra = 39.4$ and 40, the heat transfer process within the porous cavity is essentially conductive. The two other cases chosen were motivated by the critical Rayleigh number proposed by Zezib and Kassoy [8], of $4.5\pi^2$ (approximately $Ra = 44.4$), for the onset of a three-dimensional convective regime. However, for both $Ra = 44$ and 45, the convective regime already dominates, in both cases with unicellular three-dimensional structure, with steady-state Nusselt numbers of 1.1978 and 1.2497, respectively.

Fig. 7 then illustrates the isotherms at steady state for the three rear faces of the cavity, showing a purely conductive situation ($Ra = 39.4$) and a established convective situation ($Ra = 50$).

For the larger values of Ra, the analysis was separated in two groups for clarity, $Ra = 60$–120 and $Ra = 150$–300. Figs. 8 and 9 show typical results for these two groups, in terms of the overall Nusselt number evolution at the cavity

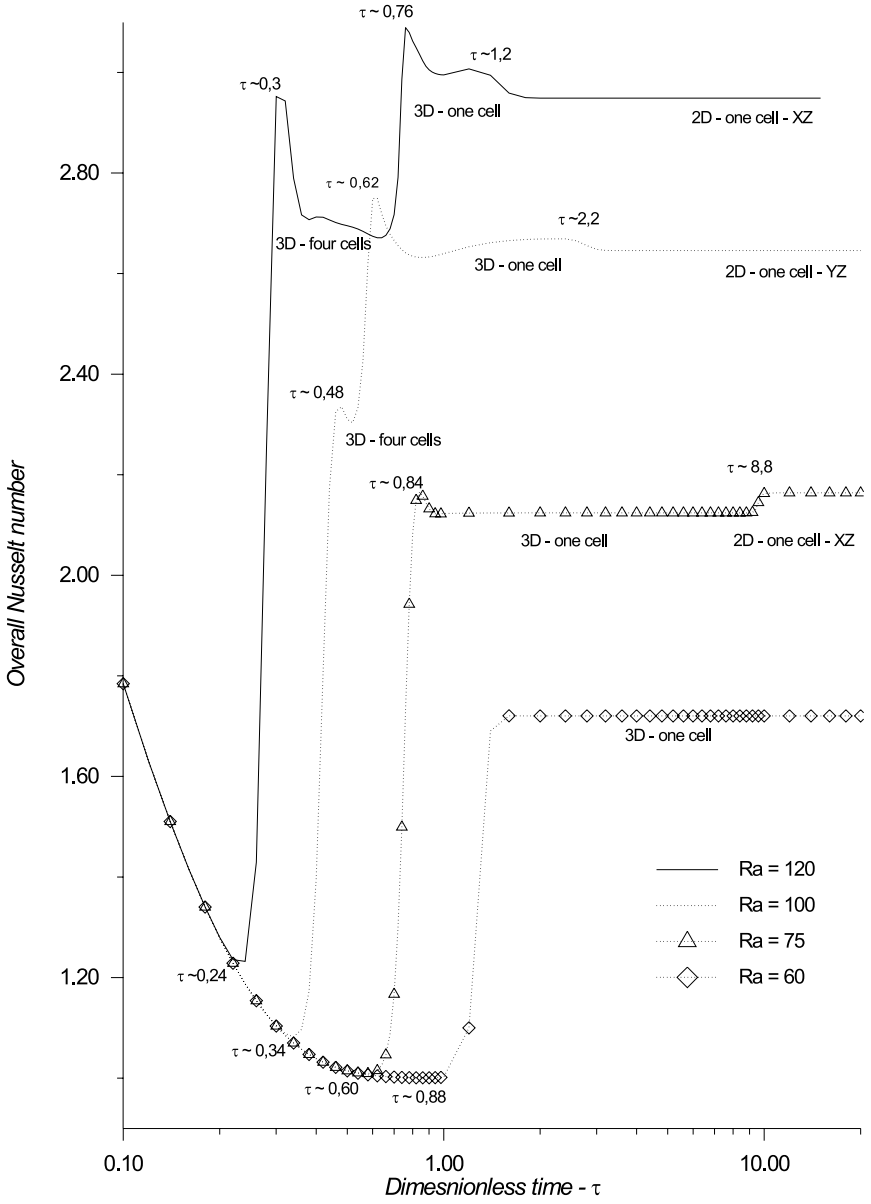

Fig. 8. Transient behavior of overall Nusselt number – cubic cavity: $Ra = 60$, 75, 100 and 120.

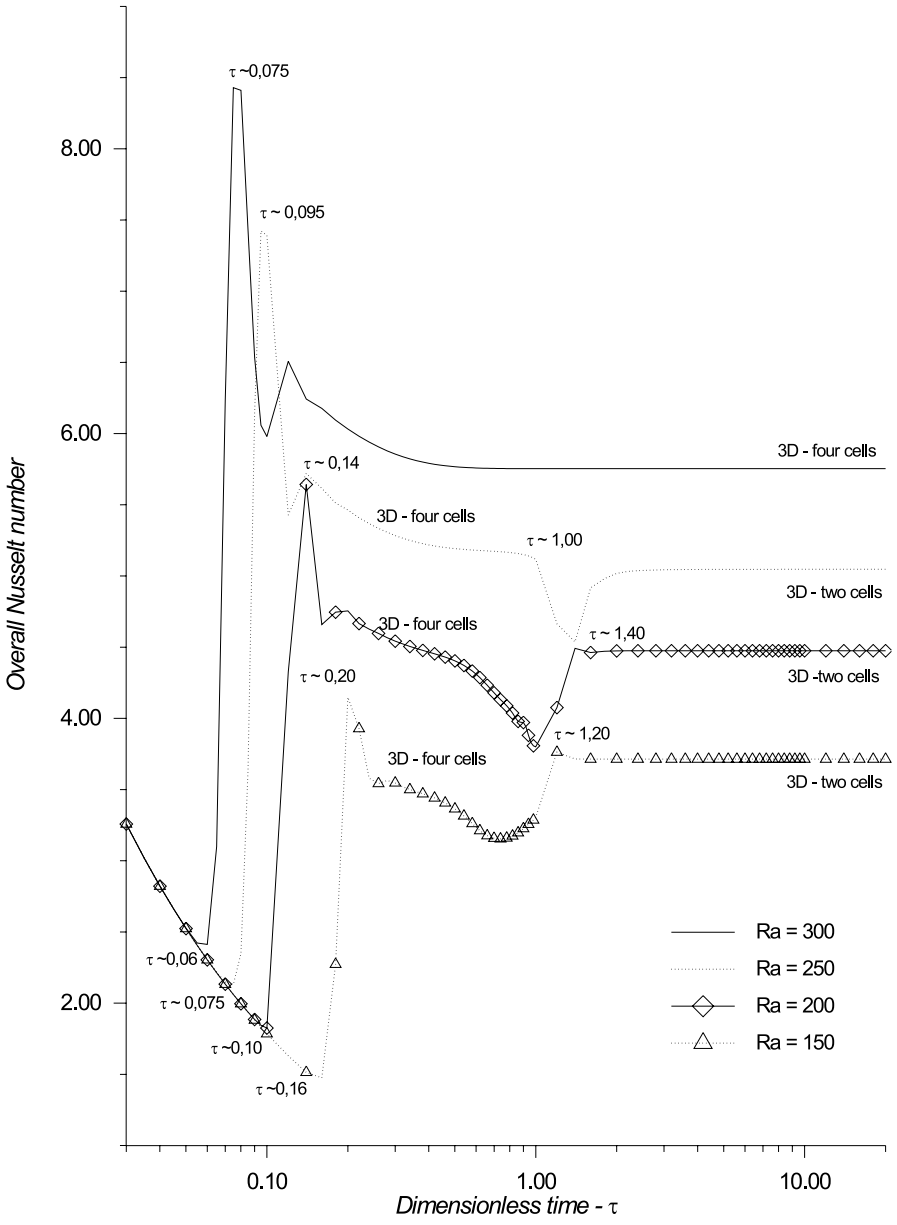

Fig. 9. Transient behavior of overall Nusselt number – cubic cavity: $Ra = 150$, 200, 250 and 300.

basis, and again the convective regime achieved are noted along the process, as made possible by visualizing the animation of the temperature results.

It can be concluded that the transition from the conductive to the convective regime can take place through distinct behaviors, according to the value of Ra, and five different patterns were observed. For instance, for $Ra = 60$ and $Ra = 75$, a unicellular three-dimensional structure is first established, which evolves in the second case to a unicellular two-dimensional pattern in the XZ plane, which results in higher heat transfer rates. For $Ra = 100$ and $Ra = 120$, we initially have a four cells three-dimensional structure, which rapidly moves into a unicellular three-dimensional pattern, with increased heat transfer, later shifting to a steady unicellular two-dimensional structure, in the XZ and YZ planes, respectively, which transfer less heat. For $Ra = 150$, $Ra = 200$ and $Ra = 250$, initially a four cells three-dimensional regime is established, which moves into a bicellular three-dimensional behavior. Finally, for $Ra = 300$, the convection is

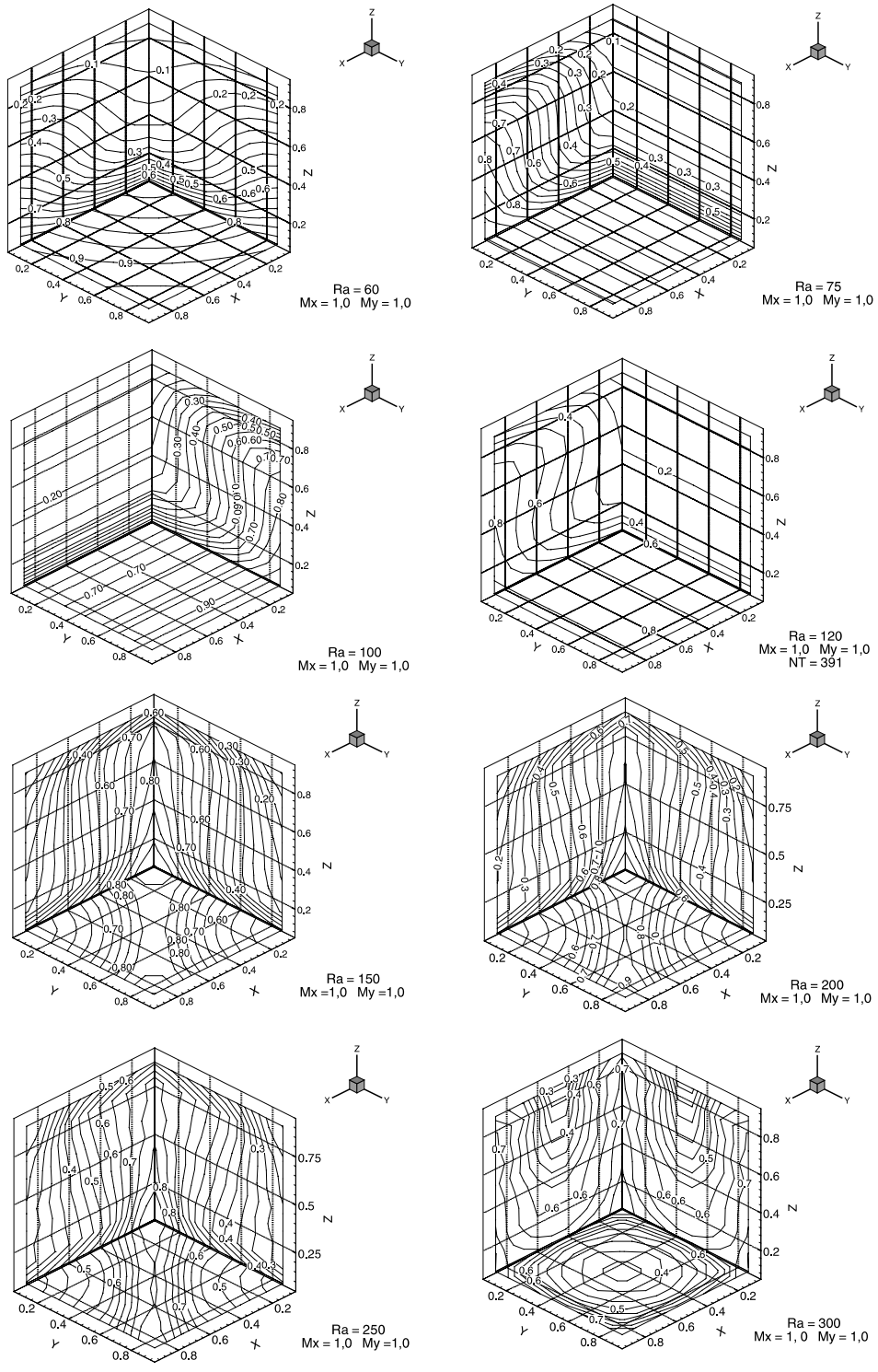

Fig. 10. Isolines of temperature at the rear faces of the cavity – steady state – cubic cavity: $Ra = 60$–300.

apparently stabilized in a four cells three-dimensional pattern. Fig. 10 consolidates the steady-state temperature behavior at the rear faces of the cavity, for all the cases considered.

The present approach was also demonstrated to be quite efficient in terms of computational effort. For instance, on a very simple configuration (microprocessor AMD K6, 266 MHz, with 128 Mb RAM), adopting $Ra = 100$ and a relative error target of 10^{-7}, a total processing time of 167 min is achieved (including file handling) with a maximum truncation order of $NT = 165$, which was more than enough to provide the desired convergence, according to the analysis illustrated in Fig. 3.

6. Conclusions

A hybrid numerical–analytical approach is proposed for the solution of transient three-dimensional coupled heat and fluid flow in natural convection within porous media, based on the ideas of the Generalized Integral Transform Technique and using the vorticity-vector potential formulation.

The limitations of the adopted Darcy flow model in predicting the transient heat transfer behaviors are discussed, and a thorough validation of the proposed algorithm is undertaken. The code constructed allowed for the qualitative analysis of the transient phenomena in terms of the Rayleigh number for the situation of cubic cavities, identifying the convective regime flow structures formed along time in each case. A set of reference results for the stabilized overall Nusselt numbers is also provided.

The combined use of a modern symbolic manipulation system [37] allowed for a substantial reduction on analysis effort and uncertainty, while providing automatic Fortran code generation for the coefficients analytical expressions in the ODE system.

The analysis should now proceed towards the consideration of more general flow models, especially accounting for the transient term in the flow equations, as already accomplished through the same approach under the two-dimensional model [29,42], finally yielding the detailed analysis of unstable buoyancy induced flows [42].

Acknowledgements

The authors would like to acknowledge the incentive of Dr. Atílio Travalloni, former Director of the Insituto Nacional de Tecnologia, INT/Brazil, for supporting the conclusion of this joint research. The partial financial support provided by CNPq/CTPETRO, FAPERJ, PRONEX and CAPES/COFECUB, all of them sponsoring agencies in Brazil, is also sincerely acknowledged.

References

[1] D.A. Nield, A. Bejan, Convection in Porous Media, Springer, New York, 1992.
[2] J. Bear, Dynamics of Fluids in Porous Media, American Elsevier, New York, 1975.
[3] M. Kaviany, Principles of Heat Transfer in Porous Media, second ed., Springer, New York, 1995.
[4] P.H. Holst, K. Aziz, Transient three-dimensional natural convection in confined porous media, Int. J. Heat Mass Transfer 15 (1971) 73–99.
[5] J.L. Beck, Convection in a box of porous material saturated with fluid, Phys. Fluids 15 (1972) 1377–1383.
[6] J.P. Caltagirone, Thermoconvective instabilities in horizontal porous layer, J. Fluid Mech. 72 (1975) 269–287.
[7] A. Zezib, D.R. Kassoy, Onset of natural convection in a box of water saturated porous media with large temperature variation, Phys. Fluids 20 (1977) 4–9.
[8] A. Zezib, D.R. Kassoy, Three-dimensional natural convection motion in a confined porous medium, Phys. Fluids 21 (1978) 1–3.
[9] R.N. Horne, Three-dimensional natural convection in a confined porous medium heated from below, J. Fluid Mech. 92 (1979) 751–766.
[10] J.M. Straus, G. Schubert, Three-dimensional convection in a cubic box of fluid-saturated porous material, J. Fluid Mech. 91 (1979) 155–165.
[11] G. Schubert, J.M. Straus, Three-dimensional and multicellular steady and unsteady convection in fluid-saturated porous media at high Rayleigh numbers, J. Fluid Mech. 94 (1979) 25–38.
[12] J.M. Straus, G. Schubert, Modes of finite-amplitude three-dimensional convection in rectangular boxes of fluid-saturated porous material, J. Fluid Mech. 103 (1981) 23–32.
[13] Y.T. Chan, S. Banerjee, Analysis of transient three-dimensional natural convection in porous media, ASME J. Heat Transfer 103 (1981) 242–248.
[14] K.J. Beukema, S. Bruin, J. Schenk, Three-dimensional natural convection in a confined porous medium with internal heat generation, Int. J. Heat Mass Transfer 26 (1983) 451–458.

[15] S. Kimura, G. Schubert, J.M. Straus, Time-dependent convection in fluid-saturated porous cube heated from below, J. Fluid Mech. 207 (1989) 153–189.
[16] D.W. Stamps, V.S. Arpaci, J.A. Clark, Unsteady three-dimensional natural convection in a fluid-saturated porous medium, J. Fluid Mech. 213 (1990) 377–396.
[17] H. Ozoe et al., Three-dimensional natural convection in a porous media at a rectangular corner, Numer. Heat Transfer, Part A 17 (1990) 249–268.
[18] A.S. Dawood, P.J. Burns, Steady three-dimensional convective heat transfer in a porous box via multigrid, Numer. Heat Transfer, Part A 22 (1992) 167–198.
[19] A.K. Singh, E. Leonardi, G.R. Thorpe, Three-dimensional natural convection in a confined fluid overlying a porous layer, ASME J. Heat Transfer 115 (1993) 631–638.
[20] K. Aziz, J.D. Hellums, Numerical solution of three-dimensional equations of motion for laminar natural convection, Phys. Fluids 10 (1967) 314–324.
[21] G.J. Hirasaki, J.D. Hellums, A general formulation of the boundary conditions on the vector potential in three-dimensional hydrodynamics, Quart. J. Appl. Math. 26 (1968) 331–342.
[22] G.J. Hirasaki, J.D. Hellums, Boundary conditions on the vector and scalar potentials in viscous three-dimensional hydrodynamics, Quart. J. Appl. Math. 28 (1970) 293–296.
[23] R.M. Cotta, Integral Transforms in Computational Heat and Fluid Flow, CRC Press, Boca Raton, FL, 1993.
[24] R.M. Cotta, M.D. Mikhailov, Heat Conduction – Lumped Analysis, Integral Transforms, Symbolic Computation, Wiley/Interscience, UK, 1997.
[25] R.M. Cotta (Ed.), The Integral Transform Method in Thermal and Fluids Sciences and Engineering, Begell House, New York, 1998.
[26] R. Serfaty, R.M. Cotta, Hybrid analysis of transient non-linear convection–diffusion problems, Int. J. Numer. Meth. Heat Fluid Flow 2 (1992) 55–62.
[27] A.R. Almeida, R.M. Cotta, Integral transform methodology for convection–diffusion problems in petroleum reservoir engineering, Int. J. Heat Mass Transfer 38 (1995) 3359–3367.
[28] C. Baohua, R.M. Cotta, Integral transform analysis of natural convection in porous enclosures, Int. J. Numer. Meth. Fluids 17 (1993) 787–801.
[29] L.S.B. Alves, R.M. Cotta, Transient natural convection inside porous cavities: hybrid numerical–analytical solution and mixed symbolic–numerical computation, Numer. Heat Transfer, Part A 38 (1) (2000) 89–110.
[30] M.A. Leal, J.S. Perez Guerrero, R.M. Cotta, Natural convection inside two-dimensional cavities: the integral transform method, Commun. Numer. Meth. Eng. 15 (1999) 113–125.
[31] M.A. Leal, R.M. Cotta, Steady and transient integral transform solutions of natural convection in enclosures, in: Proc. ICHMT Int. Symp. on Computational Heat Transfer, Begell House, Turkey, May 1997, pp. 418–432.
[32] H.A. Machado, M.A. Leal, R.M. Cotta, A flexible algorithm for transient thermal convection problems via integral transforms, in: Proc. Int. Symp. on Computational Heat and Mass Transfer, Keynote Lecture, North Cyprus, Turkey, April 1999, pp. 13–31.
[33] M.A. Leal, H.A. Machado, R.M. Cotta, Integral transform solutions of transient natural convection in enclosures with variable fluid properties, Int. J. Heat Mass Transfer 43 (2000) 3977–3990.
[34] J.S. Perez Guerrero, R.M. Cotta, Benchmark integral transform results for flow over a backward-facing step, Comput. Fluids 25 (1996) 527–540.
[35] J.N.N. Quaresma, R.M. Cotta, Integral transform method for the Navier–Stokes equations in steady three-dimensional flow, in: Proc. 10th ISTP – Int. Symp. on Transport Phenomena, Kyoto, Japan, November, 1997, pp. 281–287.
[36] S. Wolfram, The Mathematica Book, fourth ed., Wolfram Media, Cambridge, 1999.
[37] H. Luz Neto, Transient three-dimensional natural convection in porous media – hybrid solutions via integral transformation, D.Sc. Thesis (in Portuguese), COPPE/UFRJ, Universidade Federal do Rio de Janeiro, Rio de Janeiro, Brazil, 2000.
[38] M.D. Mikhailov, R.M. Cotta, Ordering rules for double and triple eigenvalues in the solution of multidimensional heat and fluid flow, Int. Commun. Heat Mass Transfer 23 (1996) 299–303.
[39] E.J. Correa, R.M. Cotta, H.R.B. Orlande, On the reduction of costs in eigenfunction expansions multidimensional diffusion problems, Int. J. Numer. Meth. Heat Fluid Flow 7 (1997) 675–695.
[40] IMSL Library, MATH/LIB, Houston, TX, 1989.
[41] L.S.B. Alves, H. Luz Neto, R.M. Cotta, Parametric analysis of the streamfunction time derivative in the Darcy-flow model for transient natural convection, in: Proc. 2nd International Conference on Computational Heat and Mass Transfer, CHMT-2001, Rio de Janeiro, Brazil, October 2001 (CD Rom).
[42] L.S.B. Alves, R.M. Cotta, J. Pontes, Stability Analysis of Natural Convection in Porous Cavities Through Integral Transforms, Int. J. Heat Mass Transfer 45 (2002) 1185–1195.